Civil Engineering Infrastructures Journal xx,xx
DOI: 10.22059/ceij.2024.372257.2010

Lightweight Fiberglass Concrete Beams of Varying Steel Reinforcement and Shear-Span Depth Ratios

Amr Ghoniem [1*], Mariam Gamal [2], and Louay Aboul Nour [3]

[1] Lecturer, Structural Engineering Department, Faculty of Engineering, Zagazig University, Postal Code: 44519, Egypt; https://orcid.org/0000-0003-0276-7443
* Corresponding author, *E-mail*: agghoneim@zu.edu.eg
[2] Researcher, Structural Engineering Department, Faculty of Engineering, Zagazig University, Postal Code: 44519, Egypt; gmariam446@gmail.com
[3] Professor, Structural Engineering Department, Faculty of Engineering, Zagazig University, Postal Code: 44519, Egypt; laran@zu.edu.eg

Received: 06/02/2024
Revised: 24/06/2024
Accepted: 08/07/2024

Abstract

Fiberglass lightweight concrete combines the advantages of fiber usage in a lightweight concrete matrix. In the present study, 8% of the cement weight was replaced by silica fume. Six specimens containing 2% glass fiber and 75% coarse aggregate replaced with lightweight expanded clay were subjected to a ٤-point bending test. The study examined how four shear-span depth ratios (1.5, 3.0, 3.57, and 4.5) and three reinforcement ratios (low, medium, and high) affected collapse performance. Among all low-reinforced samples, the 1.5 shear-span

depth exhibited the greatest improvements in resistance, mid-span deflection, stiffness, energy absorption, fracture energy, and toughness, showcasing flexural compression collapse. In contrast, the 3.57 shear-span depth low-reinforced specimen achieved the highest ductility ratio. Compared with all other 3.57 ratio samples, the low-reinforcement sample exhibited mixed flexural-shear crack patterns and the highest ductility ratio, fracture energy, and capacity of energy absorption. However, the highly reinforced sample displayed an oblique shear collapse mode and the highest stiffness enhancement. Finally, the proposed model predicting the shear strength was conducted. So, engineers can adapt the structural role of the fiberglass lightweight concrete beams to meet specific project requirements.

KEYWORDS. ductility; fiberglass; LECA; reinforced beams behavior; stiffness

1. Introduction

Fiberglass lightweight concrete (FLC) has attracted significant attention in the construction industry over the past decade because of its low density, long durability, and excellent thermal and acoustic insulation properties. Owing to its low weight, recent studies have shown that lightweight concrete is one of the best alternatives to traditional concrete in high-rise buildings and long-span construction. Lightweight concrete reduces member size, dead loads on construction, and total cost (Deifalla et al. 2020). Lightweight concrete is made by replacing or mixing normal aggregate with a lighter one derived from two main sources: (i) natural such as scoria and pumice. (ii) artificial such as lightweight expanded clay aggregate (LECA) and expanded shales (Kumar and Srivastava 2023).

To highlight its suitability as a sustainable structural alternative to conventional concrete for construction practices, lightweight concrete must achieve safety and serviceability by providing sufficient strength and controlling deformation under different loads. Reinforcing elements with longitudinal bars and fibers manages crack characteristics, ensuring the necessary ductility (Vakili et al. 2019). Glass fibers provide exceptional stiffness, strength, and chemical resistance (Sathishkumar et al. 2014) and are also effective in controlling shrinkage cracking (Mirza and Soroushian 2002).

Fiberglass lightweight concrete offers numerous benefits in terms of sustainability and environmental impacts. The use of glass fibers in composites contributes to the reduction of waste generated by the glass industry (Karuppannan Gopalraj and Kärki 2020). In addition, the inclusion of LECA lowers the consumption of natural resources, such as sand and gravel (Bozorgmehr Nia and Nemati Chari 2023). Aboul-Nour et al. (2023) investigated how different LECA ratios and glass fiber contents affect the density, workability, compression, and split tensile strengths of lightweight concrete. They found that a mix of 2% glass fiber and 75% replaced LECA exhibited the highest compression strength, while a mix of 1% glass fiber

showed the greatest tensile strength (Aboul-Nour et al. 2023).

Prestressed glass fiber lightweight concrete girders demonstrated a 20% weight reduction and effectively prevented bond-slip damage due to a ridged interface (Li et al. 2024). Several studies have examined the capacity of steel fiber lightweight concrete girders (Li et al. 2019; Li et al. 2021). Increasing the content of steel fibers shifts collapse modes from shear collapse to ductile flexural shear collapse, while shear resistance decreases as the shear-span depth ratio increases (Jiao et al. 2017). However, there is a gap in the experimental studies on the performance of longitudinally reinforced fiberglass lightweight concrete specimens. This study enhances the understanding of designing and optimizing FLC beams. For structural engineers, a comprehensive grasp of shear-span and reinforcement ratios is essential for accurate analysis and design.

In the current study, the results of testing six large-scale reinforced concrete specimens with constant fiber volume fraction and LECA content are presented to explore the significance and implications of the shear-span and reinforcement ratios. The specimens undergo 4-point loading tests controlled by displacement. The cracking patterns and performance parameters including the stiffness, ductility, capacity of energy absorption, toughness, and fracture energy of the FLC beam are discussed. To ensure a reliable design, the results are compared with mathematical model results. The finest model for predicting FLC beam shear strength is identified from the proposed model, six code-of-practice provisions, and seven equations from the literature.

2. Materials & methods

2.1 Test program

Concrete mixes included cement, sand as a fine aggregate, coarse normal & lightweight aggregates, tap water, silica fume (SF), superplasticizer, and glass fiber. The quantities used in the mixes are summarized in **Table 1**. The natural siliceous sand of a 1738 kg/m^3 bulk density used in our experiments had a fineness modulus of 2.72. The crushed dolomite aggregate had a

14 mm maximum size, 1570 kg/m^3 bulk density, 2.62 specific gravity, and a 2.35% water absorption ratio. ALEX Hydroponics Company locally produces LECA brown pellets, which is a coarse lightweight aggregate fired in a rotary kiln at temperatures ranging from 950 to 1100 °C. The maximum nominal size of the LECA was 20 mm, its specific gravity was 1.6, its bulk density was 1000 kg/m^3, and its water absorption ratio was 16.69. The chemical components of LECA were SiO_2 (61.12%), Al_2O_3 (18.77%), Fe_2O_3 (14.21%), CaO (1.78%), MgO (2.37%), and Loss (0.4%). **Table 2** presents a sieve analysis of the aggregates used in our study. **[Table 1 and Table 2 near here]**

In the current study, the ratio of water to cementitious materials (w/b) is set at 0.36. The study used type I Portland cement (CEMI 42.5N) to comply with Egyptian standards ES 4756-2 / 2020 and ASTM C150/C150M-22. Cementitious materials and water-reduction admixtures were used to enhance the concrete fresh and hardened characteristics. The study employed sika fume of a 0.65±0.1 kg/L density at 8% of the cement weight manufactured by Sika Egypt and MasterRheobuild1100 super-plasticizer at a rate of 2.2 Liters per 100 kg of cement. At 25 °C, the dark brown liquid MasterRheobuild1100 had a specific gravity from 1.19 to 1.26 and a pH from 6 to 11. The research used Type E glass fiber 12 mm long, 13 µm wide, and tensile strength from 500 to 600 N/mm^2 from the Egyptian European Steel Fiber Company.

The LECA was immersed for 24 hours in water to ensure saturation of the internal voids. The LECA was then removed from the water an hour before its use. All dry components, including sand, dolomite, LECA, cement, and SF, were distributed uniformly in the mixer for two minutes. Half of the mixing water was added to the water reducer and the other half was added directly to the mix. After two minutes of mixing all these components, the mix was sprinkled with fibers. Finally, hand mixing is performed to ensure the homogeneity of concrete.

Experimental surveys assessed the LECA's effectiveness as a partial replacement for coarse aggregate in concrete. The influence of LECA on the fresh and hardened properties of samples

containing 2% glass fiber was also examined. The samples' density, workability, compression, and split tensile strengths were measured according to ASTM standards (ASTM-C143/C143M-20 2020), (ASTM-C642-21 2021), (BS-EN-12390-3 2019), and (ASTM-C496/C496M-17 2017), respectively. The changes in physical and mechanical properties compared with a control mix without LECA is presented in **Table 3**. **[Table 3 near here]**

Using LECA to replace 75% of the coarse aggregate resulted in the smallest weight reduction of 16.14% compared with normal concrete. However, higher LECA content diminished compression strength. The 75% LECA mix, identified as optimal, achieved the highest strength-to-weight ratio of 3.46 MPa/kg, with a density of 2028 kg/m³, categorizing it as lightweight according to ACI definitions, which classify normal-weight concrete as having a density of 2240 to 2420 kg/m³. Additionally, the compression strength of the LECA concrete met the required standards, as structural lightweight concrete should exceed 15 MPa at 28-days per ASTM C330 and ACI-213R, 1987 guidelines.

The 75% LECA concrete revealed an experimental split tensile strength of 1.6 MPa. Wang and Wang 2013, Sajedi and Shafigh 2012, and ACI-318-2019 take into account the influence of glass fiber on strength as (f_{st} = 3.898+2.08V_f), (f_{st} = 0.5245+0.0761f_{cu}), and (f_{st} = 0.23$f_c^{0.7}$) that equals 3.9 MPa, 3.35 MPa, and 2.5 MPa for current study mix, respectively. The experimental split tensile strengths were approximately 59%, 52%, and 36% lower than the theoretical values for normal aggregate concrete calculated by Wang and Wang 2013, Sajedi and Shafigh 2012, and ACI-318-2019, respectively (Sajedi and Shafigh 2012; Wang and Wang 2013; ACI-318 2019).

2.2 Test specimens

The experimental study examined the structural attitude of LECA concrete specimens by testing girders at various shear-span depth ratios (a/d). The program involved the fabrication and testing of six reinforced concrete specimens, detailed in **Table 4**, with rectangular cross-

sections has 10 cm width and 15 cm depth, a 160 cm total length, and a 150 cm supported length. Each specimen comprised 75% LECA as a replacement for normal-weight coarse aggregates and 2% glass fiber. Specimens were labeled "L" followed by numbers indicating the shear-span depth ratio and the reinforcement bar diameter. Four specimens featured 10 mm bottom tensile reinforcement bars (low reinforcement ratio), including one control specimen with a shear-span depth ratio of 3.57, and three others at ratios of 1.5, 3.0, and 4.5. The remaining two specimens, under a ratio of 3.57, had 12 mm and 16 mm bottom tensile bars, representing medium and high reinforcement ratios. **Figure 1** illustrates the reinforcement specifics. A linear variable displacement transformer (LVDT) and a load cell measured the mid-span displacement and total applied load, respectively. The tensile longitudinal reinforcements (10 mm, 12 mm, and 16 mm) had a f_y/f_{ult} ratio of 40/60. Upper longitudinal reinforcement and stirrups were made of ordinary mild steel with an 8 mm diameter and a strength of f_y/f_{ult} = 24/35. **[Table 4 near here] [Figure 1 near here]**

3. Results & discussion

3.1 Load-Deflection relationship

Figure 2.a depicts the relationship between applied load and deflection for various samples with differing shear-span depth ratios. Generally, loading increased until collapse, exhibiting a linear nature before cracking. The curve's slope changed after cracking, indicating decreased stiffness until tensile steel yielded. Specimens with shear-span depth ratios of 4.5, 3.57, and 3.0 displayed similar load-deformation responses before and after cracking, differing only in the initial curve segment. Sample L3.57-R10 reached the curve's inflection point earlier than the others, followed by the sample with a 4.5 ratio, then the 3.0 ratio sample. Consequently, L3.57-R10 had the lowest stiffness compared with L4.5-R10 and L3-R10. After recording the ultimate load, sample L1.5-R10 showed several changes in inclination as strength increased and then declined, retaining the highest stiffness among all samples. The findings indicate that reducing

the shear-span depth ratio significantly enhanced the flexural stiffness of FLC beams.

Figure 2.b illustrates load vs. mid-span deflection for specimens with varying reinforcement ratios. Loading increased for all girders, resulting in a linear pre-cracking curve. The slope decreased after cracking, indicating reduced stiffness until tensile steel failed. The low-reinforcement ratio sample, L3.57-R10, reached the curve's inflection point before the other samples. It exhibited a minor strength increase after yielding, followed by a nearly flat plateau and a slight strength decrease. The load-deflection curve for the medium reinforcement ratio sample, L3.57-R12, consisted of two segments connected at the maximum load point, showing a sharp drop in slope post-inflection, indicating stiffness reduction. The high-reinforcement ratio sample (L3.57-R16) also experienced a sudden strength drop after reaching maximum load. These findings suggest that rising the steel reinforcement ratio improved the total stiffness of the specimens, aligning with previous research on LECA concrete containing varying amounts of steel and polypropylene fibers (Al-Khafaji and Harba 2023). **[Figure 2 near here]**

3.2 Crack pattern & collapse mode

(1) Influence of the shear-span depth ratio

Figure 3 shows the specimens' crack patterns and collapse modes with varying shear-span depth ratios: L1.5-R10, L3-R10, L3.57-R10, and L4.5-R10. In the control sample L3.57-R10, an initial flexural crack arose on the tension side in the mid-span zone. As loading enlarged, an extra flexural crack developed between the initial crack and extended vertically, while an additional crack formed in the outer shear-span on the tension side, eventually reaching the load points. This sample exhibited a flexural-compression collapse mode, culminating in concrete crushing at the top compression side between the 2-points of the applied load. **[Figure 3 near here]**

During the initial loading level, the specimen with the lowest shear-span depth ratio, L1.5-R10, showed a mid-zone mild flexural crack. Diagonal crack emerged at a load of 59 kN, with more

oblique and flexural crack appearing as the load enlarged. At 76 kN, shear crack formed in the support region, leading to collapse through a diagonal shear crack at approximately 45° from the support. Previous studies on lightweight concrete girders with steel fibers support that shear-compression collapse occurs in specimens with shear-span depth ratios of 1.5 to 2.5, involving concrete crushing in the shear compression region and subsequent larger shear crack in the tension region (Li et al. 2019).

Sample L3-R10 exhibited a crack pattern and collapse mode similar to L3.57-R10, although L3.57-R10 developed more extensive flexural and oblique crack. Sample L4.5-R10 failed likewise, showing only a flexural crack in the mid-span zone, resulting in an exclusively flexural collapse followed by concrete crushing between the two loading points. While specimens with shear-span depth ratios of 3.0, 3.57, and 4.5 demonstrated similar flexural-compression collapse modes, those with ratios of 3.0 and 3.57 were in a transitional phase from shear collapse to pure flexural collapse, leading to a gradual disappearance of shear crack in favor of additional flexural crack. As the shear-span depth ratio increased, the main crack shifted from the the outer shear spans to the middle flexural bending region.

Table 5 quantitatively compares the cracking and peak loads, as well as moment resistance, for specimens with different shear-span depth ratios. The control sample (of shear-span depth ratio 3.75, L3.57-R10) exhibited its first crack at 13 kN. In contrast, the specimen with the smallest shear-span depth ratio (1.5) demonstrated superior crack resistance. At loads of 32 kN and 20 kN, L1.5-R10 and L3-R10 showed approximately 146% and 54% more resistance to the initial crack, respectively. At peak load, the control sample reached an ultimate load and resistance of 33.35 kN and 8.33 kN·m, respectively. Specimens with shear-span depth ratios of 1.5 and 3.0 (L1.5-R10 and L3-R10) surpassed the control sample's ultimate load and resistance by approximately 141% and 33.4%, peaking at 80.5 kN, 20.14 kN·m, and 44.51 kN, 11.12 kN·m. Additionally, the sample with a lower shear-span depth ratio (1.5) exhibited the greatest

deflection at 16.11 mm, while deflection decreased to 12.28 mm and 10.34 mm for specimens with ratios of 3.0 and 3.57, respectively. The deflection of the 4.5 shear-span depth ratio specimen slightly increased to 10.76 mm. **[Table 5 near here]**

Consequently, specimens with lower shear-span depth ratios displayed superior anti-cracking performance, indicated by increased cracking deflection and load, as shown in **Figure 4.a** and **Figure 4.c**. Hence, reducing the shear-span depth ratio enhanced ultimate resistance and deflection, as illustrated in **Figure 4.b** and **Figure 4.d**. This finding aligns with Sathiyamoorthy's assertion that lightweight girder shear resistance increases as the shear-span depth ratio decreases (Sathiyamoorthy 2021). As this ratio reduces, compression struts can effectively transfer internal forces directly to supports through arch action. The specimen with the highest shear-span depth ratio (L4.5-R10) experienced a delay of approximately 24.5% in its first cracking load compared with the control sample. Despite a higher shear-span depth ratio, L4.5-R10 had a lower ultimate load and resistance of about 2.9%. Yin and Hu (2021) noted that the increase in cracking load is attributed to the load transfer mechanism (Yin and Hu 2021). **[Figure 4 near here]**

(2) Influence of the tensile steel

Figure 5 illustrates crack patterns and collapse modes of established specimens with a constant shear-span depth ratio and varying reinforcement ratios L3.57-R10, L3.57-R12, and L3.57-R16. For L3.57-R12, a minor flexural crack arose at a 26 kN loading. At 29 kN, an oblique crack formed near the 2-points of loading, leading to diagonal shear-compression collapse characterized by a substantial crack under the loading point and compression concrete crushing. Specimen L3.57-R16 exhibited similar diagonal shear-compression collapse but with more crack before the collapse, particularly in the mid-span zone. As the load increased, an oblique crack propagated on the tensile side, with a minor shear crack appearing near the supports at 53 kN. Both L3.57-R12 and L3.57-R16 experienced local failures due to stress concentrations at

the supports. **[Figure 5 near here]**

This crack pattern was linked to the formation of fractures and the nonlinear nature of concrete materials. The tensile reinforcement diameters for 12 mm and 16 mm exceeded the maximum tensile reinforcement ratio (ρ_{max}), while the 10 mm diameter was below it. According to ACI 318, reinforcement ratios were as follows: minimum (ρ_{min}) 0.3, maximum (ρ_{max}) 1.33, and balanced (ρ_b) 1.77, indicating that to ensure ductile collapse, specimens should be under-reinforced ($\rho_b<\rho<\rho_{min}$) (ACI-318 2019). Enlarging the steel reinforcement ratio beyond ρ_{max} shifted the collapse mode to undesirable shear-compression collapse, consistent with findings by (Alhassan et al. 2017).

Specimens with medium and high reinforcement ratios showed deflections of 6.6% and 3% less at maximum load than those with low steel reinforcement ratios, aligning with Shafigh et al. (2011), which highlighted that lighter concrete girders with lower reinforcement deflected more (Shafigh et al. 2011). Thus, higher reinforcement ratios enhance cracking resistance and deflection, delaying crack appearance (**Figure 6.a** and **6.b**). **Figures 6.c** and **6.d** demonstrate that a higher reinforcement ratio increases ultimate moment capacity without affecting maximum deflection, supporting similar results from Zhu et al. (2018) and Wang et al. (2022) (Zhu et al. 2018; Wang et al. 2022). **[Figure 6 near here]**

The high tensile reinforcement ratio specimen L3.57-R16 exhibited a 131% increase in cracking load (30.1 kN) and moment (7.52 kN.m) compared with the low reinforcement control sample. The medium reinforcement ratio L3.57-R12 showed a 63.8% increase in cracking load (21.3 kN) and moment (5.3 kN.m). The peak load and resistance also increased similarly for both medium and high reinforcement ratios, with L3.57-R12 (43.5 kN, 10.89 kN.m) and L3.57-R16 (65.2 kN, 16.3 kN.m) showing increases of 30.6% and 95.7% compared with the control sample. These trends resonate with findings by Al-Khafaji and Harba (2023), who noted the flexural capacity decrease of lightweight concrete girders as tension reinforcement diminished

(Al-Khafaji and Harba 2023).

3.3 Performance parameters

The lightweight nature of FLC makes it particularly suitable for buildings in earthquake-prone areas, reducing seismic strain while maintaining strength. Therefore, it is essential to calculate the stiffness, ductility, energy absorption capacity, toughness, and fracture energy of FLC beams. According to ACI-318-2019, the secant method is used to determine stiffness (ACI-318 2019). As shown in **Figure 7.a**, a lower shear-span depth ratio significantly reduces stiffness; it decreased by about 77.9% as the ratio increased from 1.5 to 4.5. Conversely, rising the diameter of the reinforcement steel from 10 to 12 and 16 mm improved stiffness by approximately 34.7% and 80.8%, respectively, as illustrated in **Figure 7.b**.

Ductility and energy absorption reflect the conversion of mechanical applied energy into internal potential energy within reinforced concrete elements, serving as structural safety indices (Hanoon et al. 2017). Accurate prediction of ductility is crucial for assessing a structure's ability to withstand inelastic deformations without losing its load-carrying capacity. The displacement ductility ratio, μ, was calculated using (ASTM-E2126-11 2011) equation. Among various shear-span depth ratios, the shear-collapse mode negatively affected the ductility ratio of the L1.5-R10 sample, as shown in **Figure 7.c**. Comparatively, samples L3.57-R16 and L3.57-R12 exhibited lower ductility ratios due to shear collapses versus the flexural collapse mode of sample L3.57-R10, with reductions of 61.2% and 59.6%, respectively, as demonstrated in **Figure 7.d**.

Energy absorption, determined as the area below load-deflection trajectory, remains vital for maintaining structural integrity under unusual loads. Results indicated an inverse relationship between shear-span depth ratio and capacity of energy absorption, which decreased by approximately 108.9% when increasing the ratio (1.5 to 4.5), as illustrated in **Figure 7.e**. Conversely, changing the reinforcement steel diameter from 12 mm to 16 mm resulted in

reductions of 52.9% and 27% in energy capacity, respectively. Additionally, increasing the bottom tensile reinforcement diminished energy absorption capacity, as shown in **Figure 7.f**.

[Figure 7 near here]

Fracture energy is crucial for understanding concrete behavior in large structures and shear tests. Using the equation outlined by (Gyawali 2023), the fracture energies were assessed for comparison. Sample L1.5-R10 recorded the highest fracture energy, while sample L3-R10 was 78.2% lower. **Figure 8.a** demonstrates that increasing the shear-span depth ratio to 3.57 and 4.5 reduced fracture energy by 105.6% and 108%, respectively, indicating its direct impact on energy absorption during fracture. Although no clear relationship exists between reinforcement ratio and fracture energy, samples with lower ratios showed a more significant effect on fracture energy. For samples L3.57-R16 and L3.57-R12, increasing the reinforcement ratio led to reductions in energy of approximately 26.84% and 52.62%, respectively, as depicted in **Figure 8.b**.

Yield and ultimate toughness values were derived from (ASTM-C1018 1997) equation. **Figures 8.c** and **8.e** illustrate that these values decreased by 151.91% and 3.62%, respectively, as the shear-span depth ratio increased from 1.5 to 4.5. A lower shear-span depth ratio positively influences yield and ultimate toughness, with higher yield toughness generally associated with increased initial crack loads (Safiuddin et al. 2022). The high ultimate toughness values suggest that the LECA aggregate and glass fiber mixture enhances the FLC girders' resistance to tensile stresses. A high reinforcement ratio significantly affects yield toughness positively but detracts from ultimate toughness, as shown in **Figures 8.d** and **8.f**.

Utilizing 75% expanded clay particles reduces concrete density to 2028.6 kg/m^3, thereby decreasing the dead load on structures. Furthermore, the 75% LECA concrete demonstrated acceptable compression strength (31 MPa) and split tensile strength (1.6 MPa). These combined properties make FLC ideal for applications where strength and weight are critical, such as in

high-rise construction. Despite a low reinforcement ratio, incorporating glass fibers into the concrete matrix enhanced tension capacity and improved resistance to cracking and shrinkage.

[Figure 8 near here]

3.4 Experimental result vs. theoretical estimation

The assumptions of the proposed doubly reinforced prediction model for the fibrous concrete beams shear strength include contributions from the nominal shear strength of concrete, longitudinal reinforcement, stirrups, and fibers, as defined in Eq. (1). Here, $v_{fc;u}$ represents the longitudinally steel reinforced fibrous girders ultimate shear strength, $v_{fc;st}$ indicates the stirrups shear strength, and $v_{fc;sf}$ accounts for the shear strength from the fibrous matrix, compression steel, and longitudinal bottom steel (ACI-544.4R-88 1988). **Figure 9** illustrates the nominal moment calculated using the proposed model, based on the stress and strain distributions in the fibrous concrete sample. The shear strength contribution of fibers and reinforcement steel for a doubly reinforced fibrous concrete sample, $v_{fc;sf}$, is determined as shown in Eq. (2). **[Figure 9 near here]**

$$v_{fc;u} = v_{fc;sf} + v_{fc;st} \tag{1}$$

$$v_{fc;sf} = \left[\frac{\sigma_t (h-e)}{ad}\left(\frac{h}{2}+\frac{e}{2}-\frac{x}{2}\right)\right] + \frac{f_y A_{sc}}{abd}\left(\frac{x}{2}-d'\right) \tag{2}$$

$$\sigma_t = 0.00772\frac{V_f l_f}{d_f} F_{be} \tag{3}$$

$$e = h - \frac{0.85 f_c' x}{\sigma_t} + \frac{f_y}{\sigma_t b}(A_s - A_{sc}) \tag{4}$$

$$c = \frac{\varepsilon_c d}{\varepsilon_c + \frac{f_y}{E_s}} \tag{5}$$

In the equations, σ_t denotes the tension stress in fibrous concrete (Eq. 3), V_f is the fiber content, and l_f/d_f represents the fiber aspect ratio. F_{be}, the fiber bond effectiveness, varies from 1.0 to 1.2 based on the fiber features (set to 1.0 in this study). Parameters such as the girder total depth (h), shear span (a), girder width (b), distance from the supreme compression fiber to the center of the tension steel bars (d), depth of the rectangular stress block (x), and internal tension and

compression forces (e) are distincted in Eqs. (4) and (5). The yielding strength of the bars (f_y), the area of tension steel (A_s), the compression steel area (A_{sc}), the distance from the supreme compression fiber to the center of compression steel (d'), and the compression strength of plain concrete (f_c') are also specified. The supreme compression fiber to the neutral axis distance (c) is based on strain distribution and the concrete compression strain (ε_c) which is 0.0035 for 1.0% fiber content and 0.004 for 1-3% fiber content, with the steel elasticity modulus (E_s) equal to 200 GPa.

Theoretical models are usually considered for integration into design codes due to their simplicity and satisfactory test results for fibrous specimens. **Figure 10** compares the test shear strength values of fibrous concrete girders with those predicted by the proposed model and thirteen existing models. The models (AS-3600 2018), (ACI-544.4R 2018), (Ashour et al. 1992), (ACI-318 2019), (Eurocode-2 2004), (CECS-38 2004), (Kwak et al. 2002), (Narayanan and Darwish 1987), (Shin et al. 1994), (Imam et al. 1995), (Li et al. 2019), (JGJ12 2006), (Yi et al. 2017), and the current proposed model exhibited similar trends across samples and reasonably predicted experimental shear strength values, except for the 1.5 shear-span depth ratio sample evaluated by Eurocode 2, 2004. **[Figure 10 near here]**

The theoretical shear strength of each FLC girder that failed in shear was compared with actual measured strengths. **Table 6** presents the mean of the $v_{fc;THEO}/v_{fc;EXP}$ ratios for each model. The proposed model, AS 3600-2018, Ashour et al. 1992, ACI 318-2019, ACI 544.4R-2018, JGJ12-2006, and Yi et al. 2017 exhibited mean values close to 1.0 with a total standard deviation of less than 0.5. They demonstrated conservative estimation, with deviations of 7.19%, 7.89%, 23.44%, -35.96%, 45.60%, 52.37%, and 58.41% from experimental results. The previous seven models overestimated shear strength capacity, except ACI 544.4R-2018, which underestimated it. The equations of the AS 3600-2018 and Ashour et al. 2009 models are fundamentally similar, utilizing parameters such as f_c', A_s, f_y, b, and shear-span depth ratio, with the main distinction

being Ashour et al. 2009 including fiber pullout resistance v_b as a shear strength contribution, while ACI 544.4R-2018 does not consider longitudinal reinforcements. According to Lim et al. 2006, the American code effectively forecasts the ultimate strength of lightweight concrete girders (Lim et al. 2006).

The remaining seven models, including Eurocode 2-2004, Kwak et al. 2002, Shin et al. 1994, CECS 38-2004, Narayanan and Darwish 1987, Li et al. 2019, and Imam et al. 1995, consistently underestimated shear strength, with average $v_{fc;THEO}/v_{fc;EXP}$ values below 5.55 and standard deviations under 2, showing deviations exceeding 60% from experimental results. **[Table 6 near here]**

4. Conclusions

This research investigates the impact of the steel reinforcement ratio and shear-span depth ratio on the fiberglass lightweight concrete (FLC) beams behavior. The experimental program provides valuable insights into load capacity, deflection behavior, and fracture propagation. The important conclusions are as follows:

(1) The shear-span significantly affects the shear and load capacities of FLC girders. Increasing the shear-span depth ratio from 1.5 to 4.5 reduced shear fracture propagation while increasing flexural crack propagation until pure flexural crack developed in a low-reinforced sample at a 4.5 shear-span depth ratio.

The R10 bars beam with the smallest shear-span depth ratio of 1.5 showed enhanced cracking resistance, cracking deflection, peak resistance, peak deflection, stiffness, ductility ratio, capacity of energy absorption, fracture energy, yield, and ultimate toughness by 146%, 16%, 141%, 55.8%, 91.5%, -43.8%, 106%, 105.6%, 185.81%, and 38.57%, respectively, compared to the R10 bars beam with a 3.57 shear-span depth ratio.

Lowering the shear-span depth ratio positively impacted all performance measures except for the ductility ratio. A greater shear span can lead to excessive deflections and increased

ductility, with the main crack shifting from the exterior shear spans to the interior flexural bending region, where the girder becomes more flexible.

(2) The reinforcement ratio is vital for the load capacity and crack resistance of FLC girders. High- and medium-reinforced specimens exhibited shear-compression collapse, while the low-reinforced sample showed flexural-compression collapse.

The R16 bars high-reinforced specimen at a 3.57 shear-span depth ratio demonstrated the greatest improvements in cracking resistance, cracking deflection, peak resistance, stiffness, and yield toughness by 131%, 26%, 95.7%, 80.8%, and 191.85%, respectively, compared with the low-reinforced R10 bars specimen. However, peak deflection, ductility ratio, capacity of energy absorption, fracture energy, and ultimate toughness decreased by -3%, -61.2%, -27%, -26.84%, and -33.13%, respectively.

Higher reinforcement ratios enhance tensile strength and crack resistance, but excessive reinforcement can negatively affect the collapse mode, shifting from diagonal tension to shear-compression collapse. High reinforcement ratios may lead to insufficient crack warnings, raising significant safety concerns.

(3) Designing FLC beams with varying shear spans and reinforcement ratios necessitates careful attention to relevant design codes and standards. The results of the theoretical to experimental shear strength ratio validate the effectiveness of the current study's model and the AS 3600-2018 model in accurately predicting the shear strength of fiberglass lightweight concrete girders.

Acknowledgments

This research did not receive any specific grant from funding agencies in the public, commercial, or not-for-profit sectors.

5. References

Aboul-Nour, L., Gamal, M., and Ghoniem, A. (2023). "Glass Fiber for Improved Behavior of Light Expanded Clay Aggregate Concrete Beams: An Experimental Study", *Frattura ed Integrità Strutturale (Fracture and Structural Integrity)*, 17(65). https://doi.org/10.3221/IGF-ESIS.65.01

ACI-318 (2019). "Building Code Requirements for Structural Concrete (ACI 318-19) Commentary on Building Code Requirements for Structural Concrete (ACI 318R-19)", *American Concrete Institute ACI, Farmington Hills, United States*. https://standards.globalspec.com/std/14349342/aci-318m

ACI-544.4R-88 (1988). "Design considerations for steel fiber reinforced concrete", *American Concrete Institute, Farmington Hill, Michigan, USA*. https://standards.globalspec.com/std/1210947/aci-544-4r

ACI-544.4R (2018). "Guide to Design with Fiber-Reinforced Concrete", *American Concrete Institute, Farmington Hill, Michigan, USA*. https://standards.globalspec.com/std/13051488/aci-544-4r

Al-Khafaji, N. H. A., and Harba, I. S. I. (2023). "Shear and Flexural Behavior of Lightweight Concrete Beams Containing Hybrid Fibers", *Civil and Environmental Engineering*, 19, 206 - 217. https://doi.org/10.2478/cee-2023-0018

Alhassan, M., Al-Rousan, R., and Ababneh, A. (2017). "Flexural behavior of lightweight concrete beams encompassing various dosages of macro synthetic fibers and steel ratios", *Case Studies in Construction Materials*, 7, 280-293. https://doi.org/10.1016/j.cscm.2017.09.004

AS-3600 (2018). "Concrete Structures", *Standards Australia Limited, Sydney*. https://store.standards.org.au/product/as-3600-2018

Ashour, S. A., Hasanain, G. S., and Wafa, F. F. (1992). "Shear Behavior of High-Strength Fiber Reinforced Concrete Beams", *Aci Structural Journal*, 89, 176-184. https://doi.org/10.14359/2946

ASTM-C143/C143M-20 (2020). "Standard Test Method for Slump of Hydraulic cement Concrete", *American Society of Testing and Materials, ASTM International, West Conshohocken, Philadelphia, USA*. https://standards.globalspec.com/std/14302069/astm-c143-c143m-20

ASTM-C496/C496M-17 (2017). "Standard Test Method for Splitting Tensile Strength of Cylindrical Concrete Specimens", *American Society of Testing and Materials, ASTM*

International, West Conshohocken, Philadelphia, USA. https://standards.globalspec.com/std/4055208/astm-c496-c496m-17

ASTM-C642-21 (2021). "Standard test method for density, absorption, and voids in hardened concrete", *American Society of Testing and Materials, ASTM International, West Conshohocken, Philadelphia, USA*. https://standards.globalspec.com/std/14510464/astm-c642-21

ASTM-C1018 (1997). "Standard Test Method for Flexural Toughness and First-Crack Strength of Fiber-Reinforced Concrete (Using Beam With Third-Point Loading)", *ASTM International, USA*. https://standards.globalspec.com/std/3811416/astm-c1018-97

ASTM-E2126-11 (2011). "Standard Test Methods for Cyclic (Reversed) Load Test for Shear Resistance of Vertical Elements of the Lateral Force Resisting Systems for Buildings", *ASTM International, West Conshohocken, PA, USA*. https://doi.org/10.1520/E2126-11

Bozorgmehr Nia, S., and Nemati Chari, M. (2023). "Applied development of sustainable-durable high-performance lightweight concrete: Toward low carbon footprint, durability, and energy saving", *Results in Materials*, 20, 100482. https://doi.org/10.1016/j.rinma.2023.100482

BS-EN-12390-3 (2019). "Testing hardened concrete - Compressive strength of test specimens", *British Standard Institution London, UK*. https://standards.globalspec.com/std/13376131/bs-en-12390-3

CECS-38 (2004). "Technical Specification for Fibre Reinforced Concrete Structure", *China Association for Engineering Construction Standardization*. https://www.chinesestandard.net/PDF/English.aspx/CECS38-2004

Deifalla, A., Awad, A., Seleem, H., and Abdelrahman, A. (2020). "Investigating the behavior of lightweight foamed concrete T-beams under torsion, shear, and flexure", *Engineering Structures*, 219, 110741. https://doi.org/10.1016/j.engstruct.2020.110741

Eurocode-2 (2004). "Design of concrete structures–Part 1-1: General rules and rules for buildings", *European Committee for Standardization (CEN)*. https://standards.globalspec.com/std/10010073/aenor-une-en-1992-1-1-eng

Gyawali, T. R. (2023). "Effect of sand types and mixing procedures on the flexural behaviour of the high ductile mortar in monotonic and cyclic loadings", *Heliyon*, 9(3), e14452. https://doi.org/10.1016/j.heliyon.2023.e14452

Hanoon, A. N., Jaafar, M. S., Hejazi, F., and Abdul Aziz, F. N. A. (2017). "Energy absorption evaluation of reinforced concrete beams under various loading rates based on particle swarm optimization technique", *Engineering Optimization*, 49(9), 1483 - 1501. https://doi.org/10.1080/0305215X.2016.1256729

Imam, M. A., Vandewalle, L., and Mortelmans, F. (1995). "Shear – moment analysis of reinforced high strength concrete beams containing steel fibres", *Canadian Journal of Civil Engineering*, 22, 462-470. https://doi.org/10.1139/L95-054

JGJ12 (2006). "Technical Specification for Lightweight Aggregate Concrete Structures", *Ministry of Housing and Urban-Rural Construction of the People's Republic of China, China Building Industry Press: Beijing, China.* https://www.chinesestandard.net/PDF/English.aspx/JGJ12-2006

Jiao, C., Xu, B., Gao, J., and Wang, L. (2017). "Experiments on shear resistance of steel fiber reinforced lightweight aggregate concrete beams", *Journal of Civil Engineering and Management*, 34, 9-13. http://dx.doi.org/10.13579/j.cnki.2095-0985.2017.02.003

Karuppannan Gopalraj, S., and Kärki, T. (2020). "A review on the recycling of waste carbon fibre/glass fibre-reinforced composites: fibre recovery, properties and life-cycle analysis", *SN Applied Sciences*, 2(3), 433. https://doi.org/10.1007/s42452-020-2195-4

Kumar, R., and Srivastava, A. (2023). "Influence of Lightweight Aggregates and Supplementary Cementitious Materials on the Properties of Lightweight Aggregate Concretes", *Iranian Journal of Science and Technology, Transactions of Civil Engineering*, 47(2), 663-689. https://doi.org/10.1007/s40996-022-00935-5

Kwak, Y.-K., Eberhard, M. O., Kim, W.-S., and Kim, J. (2002). "Shear strength of steel fiber-reinforced concrete beams without stirrups", *ACI Structural Journal*, 99(4), 530-538. https://doi.org/10.14359/12122

Li, C., Zhao, M., Geng, H., Fu, H., Zhang, X., and Li, X. (2021). "Shear testing of steel fiber reinforced expanded-shale lightweight concrete beams with varying of shear-span to depth ratio and stirrups", *Case Studies in Construction Materials*, 14, e00550. https://doi.org/10.1016/j.cscm.2021.e00550

Li, S., Chen, W., Hu, J., Zhang, D., and Chen, L. (2024). "Flexural Behavior of Unbonded Prestressed Concrete Composite Beams Manufactured with Glass-Fiber-Reinforced Lightweight Aggregate Concrete and Conventional Concrete", *Iranian Journal of Science and*

Technology, Transactions of Civil Engineering, 48(4), 2031-2047. https://doi.org/10.1007/s40996-023-01297-2

Li, X., Li, C., Zhao, M., Yang, H., and Zhou, S. (2019). "Testing and Prediction of Shear Performance for Steel Fiber Reinforced Expanded-Shale Lightweight Concrete Beams without Web Reinforcements", *Materials*, 12(10). https://doi.org/10.3390/ma12101594

Lim, H., Wee, T., Mansur, M., and Kong, K. "Flexural behavior of reinforced lightweight aggregate concrete beams", *Proc., Proceedings of the 6th Asia-Pacific Structural Engineering and Construction Conference (APSEC 2006)*, 5-6.

Mirza, F. A., and Soroushian, P. (2002). "Effects of alkali-resistant glass fiber reinforcement on crack and temperature resistance of lightweight concrete", *Cement and Concrete Composites*, 24(2), 223-227. https://doi.org/10.1016/S0958-9465(01)00038-5

Narayanan, R., and Darwish, I. Y. S. (1987). "Use of steel fibers as shear reinforcement", *Aci Structural Journal*, 84(3), 216-227. https://doi.org/10.14359/2654

Safiuddin, M., Abdel‐Sayed, G., and Hearn, N. (2022). "Flexural and Impact Behaviors of Mortar Composite Including Carbon Fibers", *Materials*, 15(5). https://doi.org/10.3390/ma15051657

Sajedi, F., and Shafigh, P. (2012). "High-Strength Lightweight Concrete Using Leca, Silica Fume, and Limestone", *Arabian Journal for Science and Engineering*, 37(7), 1885-1893. https://doi.org/10.1007/S13369-012-0285-3

Sathishkumar, T., Satheeshkumar, S., and Naveen, J. (2014). "Glass fiber-reinforced polymer composites – a review", *Journal of Reinforced Plastics and Composites*, 33, 1258 - 1275. https://doi.org/10.1177/0731684414530790

Sathiyamoorthy, K. (2021). "Shear and flexural behaviour of lightweight self-consolidating concrete beams", PhD Thesis, Ryerson University. https://doi.org/10.32920/ryerson.14662374.v1

Shafigh, P., Hassanpour, M., Razavi, S., and Kobraei, M. (2011). "An investigation of the flexural behaviour of reinforced lightweight concrete beams", *International Journal of Physical Sciences*, 6(10), 2414-2421. https://doi.org/10.5897/IJPS10.550

Shin, S.-w., Oh, J.-G., and Ghosh, S. K. (1994). "Shear Behavior of Laboratory-Sized High-Strength Concrete Beams Reinforced With Bars and Steel Fibers", *SP-142: Fiber Reinforced Concrete Developments and Innovations*. https://doi.org/10.14359/3917

Vakili, S. E., Homami, P., and Esfahani, M. R. (2019). "Flexural Behavior of Lightweight Concrete Beams Reinforced with GFRP Bars and Effects of the Added Micro and Macro Fiber", *Civil Engineering Infrastructures Journal*, 52(2), 349-363. https://doi.org/10.22059/ceij.2019.277143.1557

Wang, H. T., and Wang, L. C. (2013). "Experimental study on static and dynamic mechanical properties of steel fiber reinforced lightweight aggregate concrete", *Construction and Building Materials*, 38, 1146-1151. https://doi.org/10.1016/j.conbuildmat.2012.09.016

Wang, Z., Xie, J., Li, J., Liu, P., Shi, C., and Lu, Z. (2022). "Flexural behaviour of seawater–sea sand concrete beams reinforced with GFRP bars: Effects of the reinforcement ratio, stirrup ratio, shear span ratio and prestress level", *Journal of Building Engineering*, 54, 104566. https://doi.org/10.1016/j.jobe.2022.104566

Yi, W., Ding, Y., and Chen, H. (2017). "Experimental study on shear behavior of lightweight aggregate concrete beams without stirrups", *Journal of Building Structures*, 6, 123-132. http://dx.doi.org/10.14006/j.jzjgxb.2017.06.014

Yin, Y., and Hu, S. (2021). "Effects of span-depth ratios on the energy release rate for three-point bending beams", *Engineering Fracture Mechanics*, 244, 107567. https://doi.org/10.1016/j.engfracmech.2021.107567

Zhu, H., Cheng, S., Gao, D., Neaz, S. M., and Li, C. (2018). "Flexural behavior of partially fiber-reinforced high-strength concrete beams reinforced with FRP bars", *Construction and Building Materials*, 161, 587-597. https://doi.org/10.1016/j.conbuildmat.2017.12.003

List of Figures

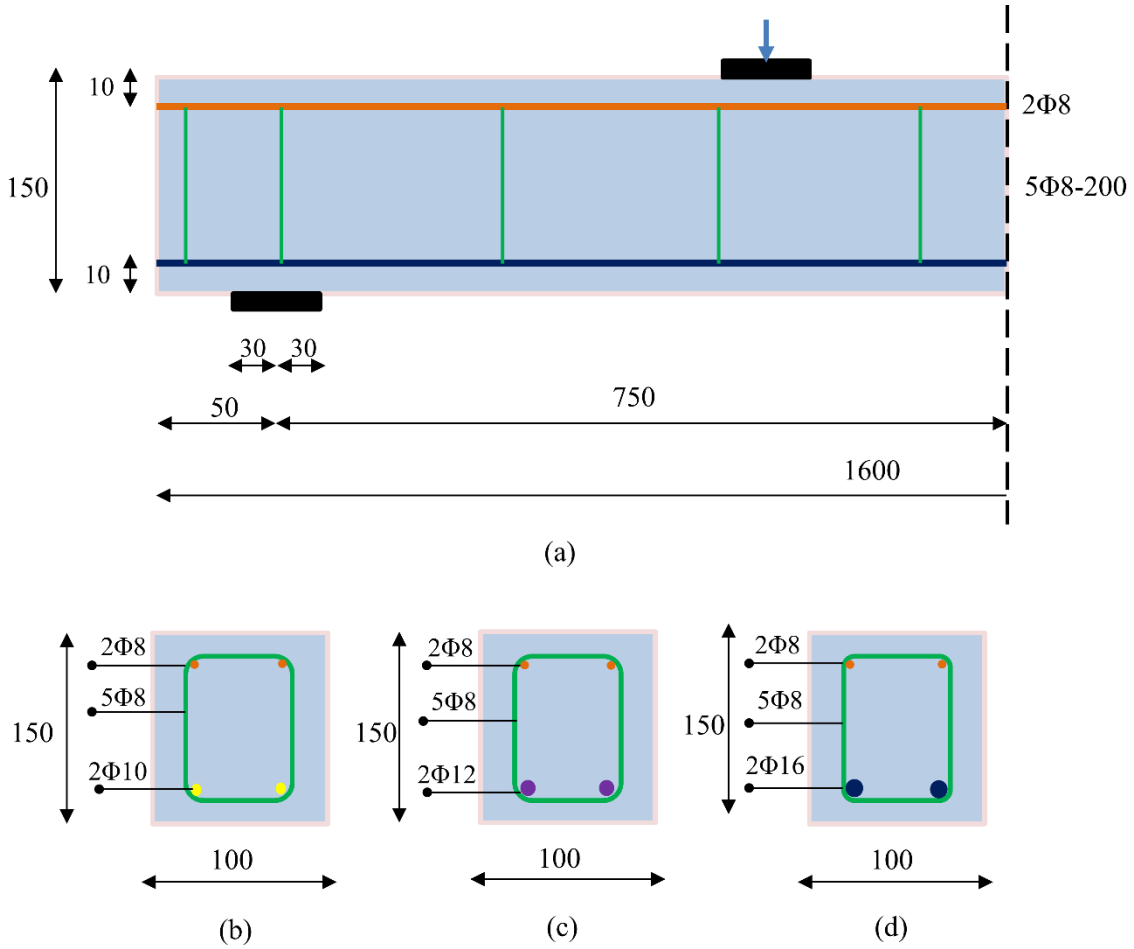

Fig. 1 Dimensions and reinforcement information of FLC beams (units: mm): (a) Half elevation of the test beam. (b) Cross section of low-reinforcement-ratio beams. (c) Cross-section of medium-reinforcement-ratio beams. (d) Cross-section of high reinforcement ratio beams.

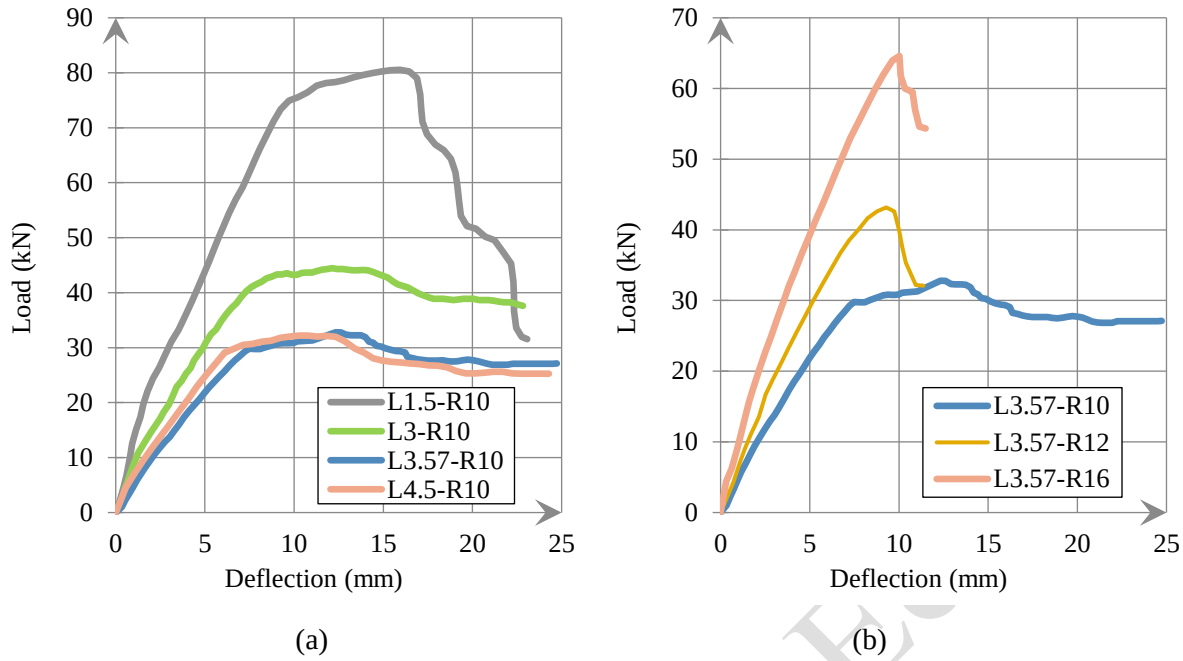

Fig. 2 Load-displacement curves for: (a) Same reinforcement and various shear-span depth ratio samples. (b) Same shear-span depth ratio and different bottom tensile reinforcement samples.

(a)

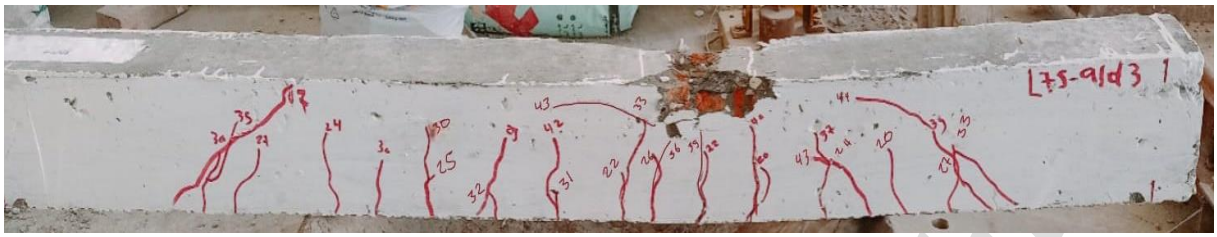

(b)

(c)

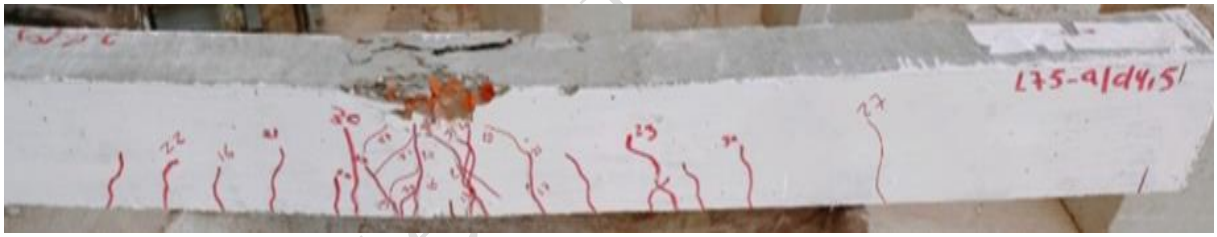

(d)

Fig. 3 Crack patterns for beams with various shear-span to depth ratios: (a) L1.5-R10. (b) L3-R10. (c) L3.57-R10. (d) L4.5-R10.

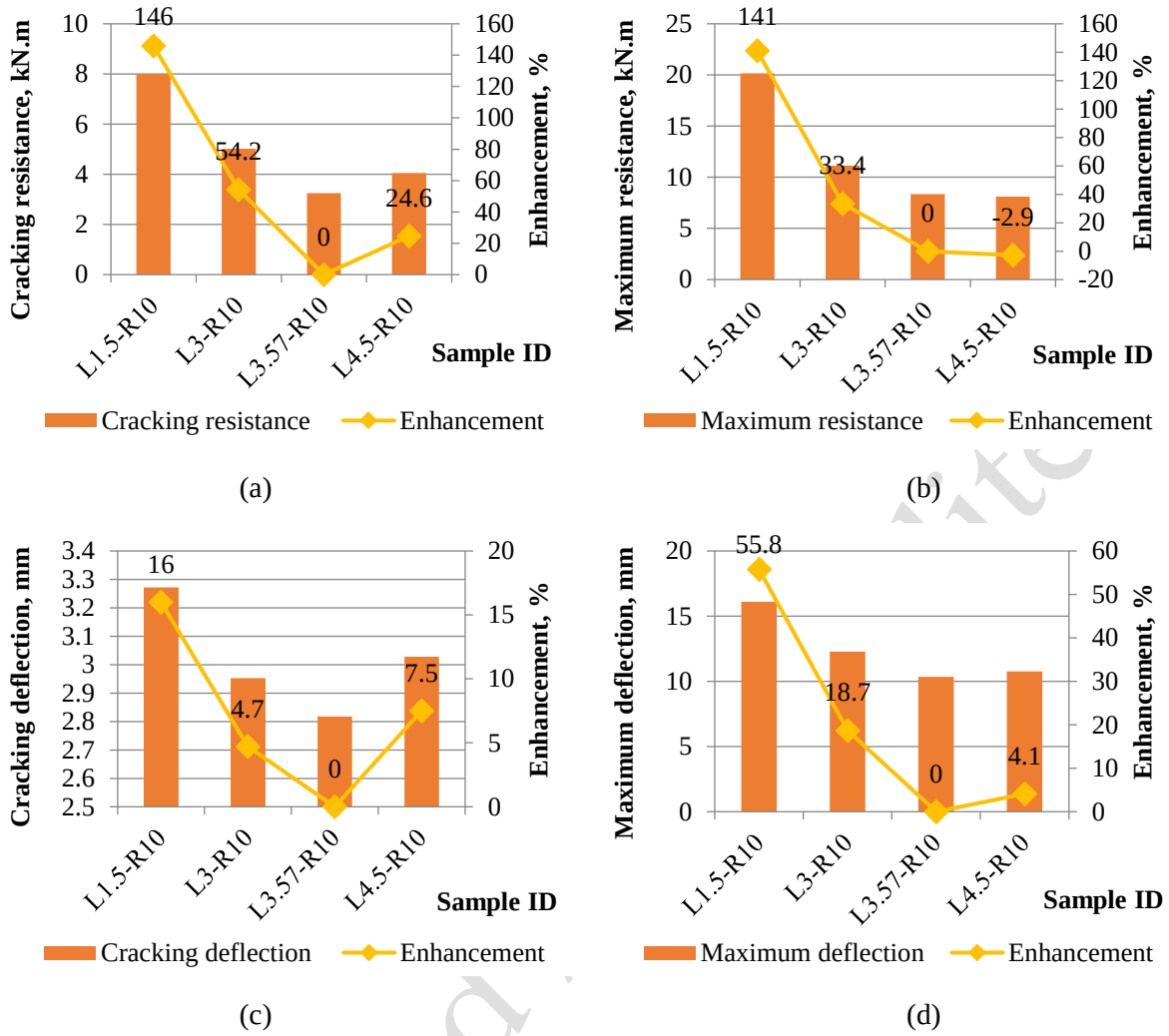

Fig. 4 Enhancement percentage of various shear-span depth ratio samples in: (a) Cracking resistance. (b) Maximum resistance. (c) Cracking deflection. (d) Maximum deflection.

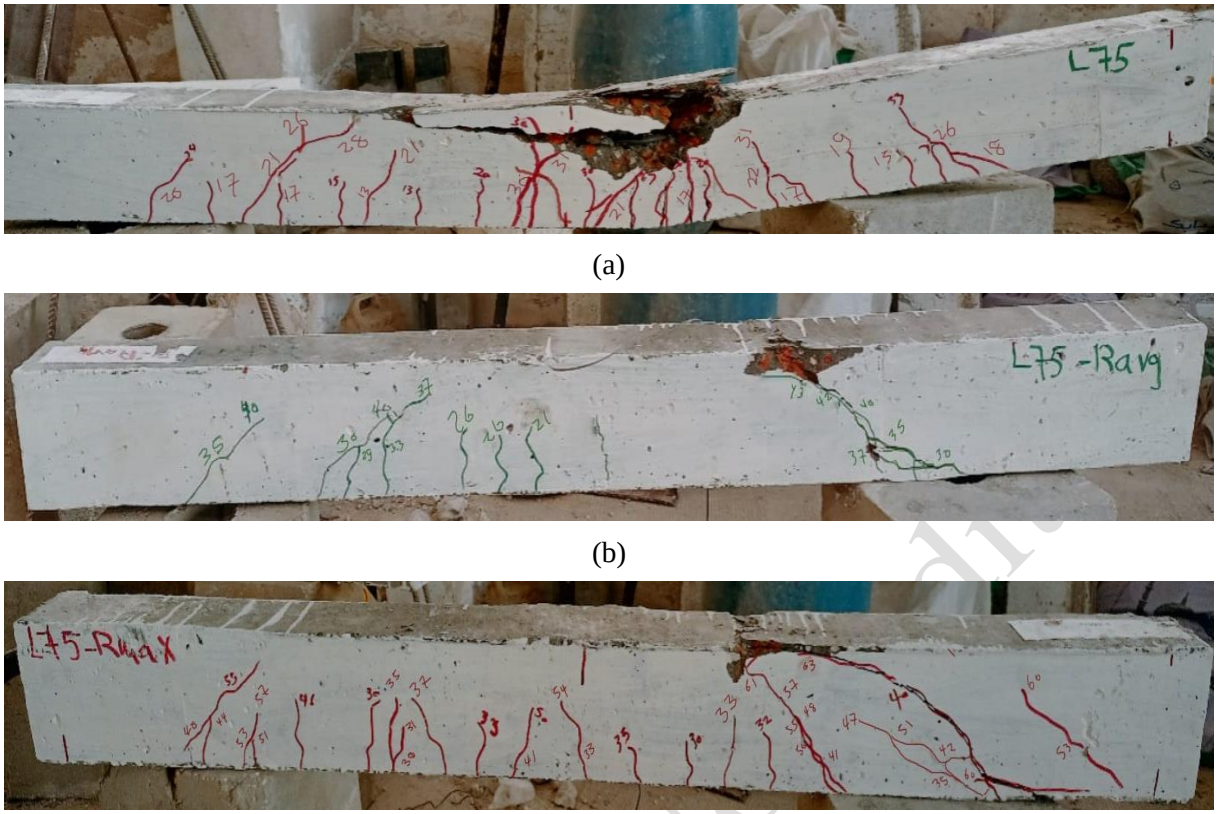

(a)

(b)

(c)

Fig. 5 Crack pattern of beams; (a) L3.57-R10. (b) L3.57-R12. (c) L3.57-R16.

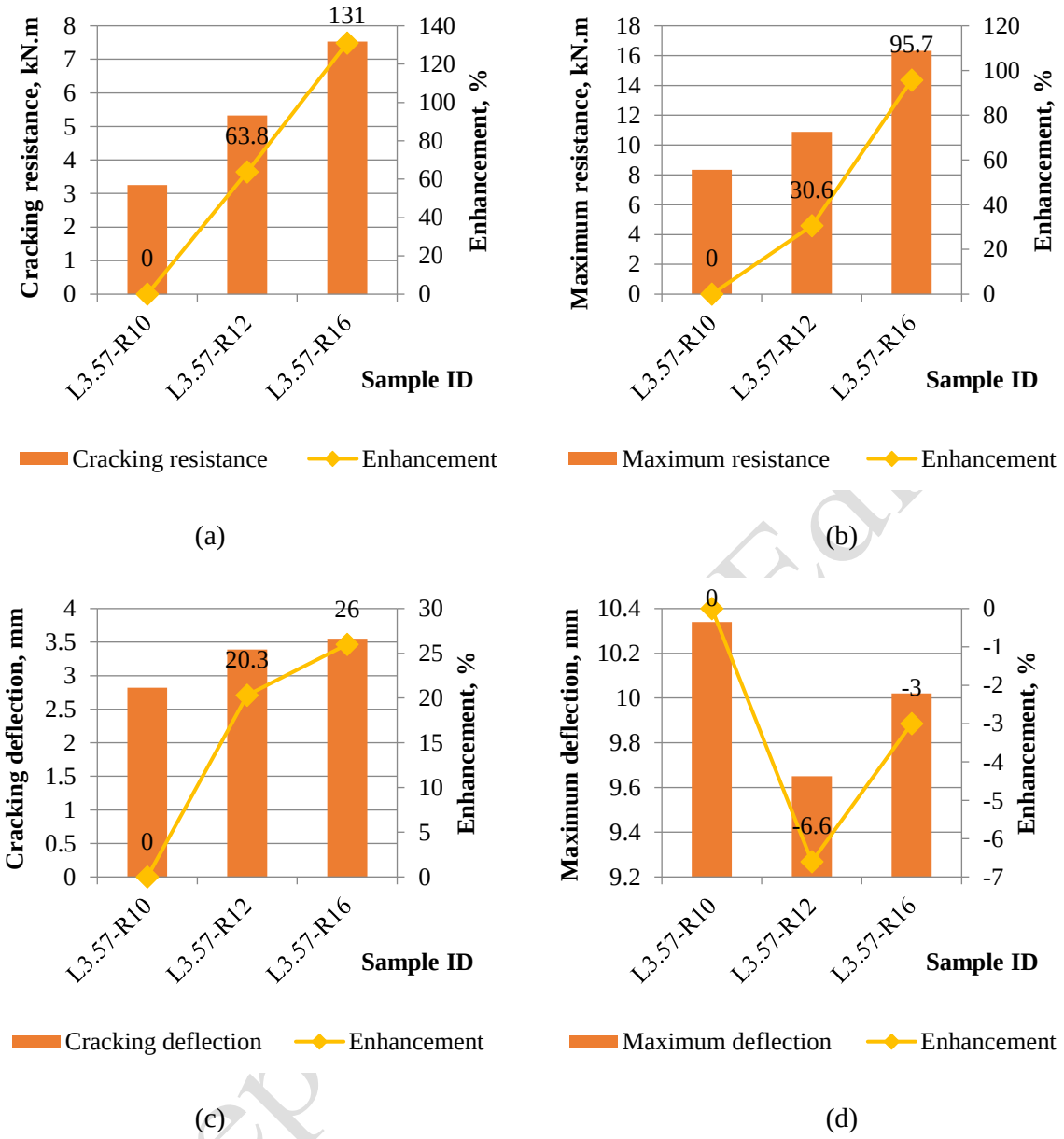

Fig. 6 Enhancement percentage of various bottom tensile reinforcement ratio samples in: (a) Cracking resistance. (b) Maximum resistance. (c) Cracking deflection. (d) Maximum deflection.

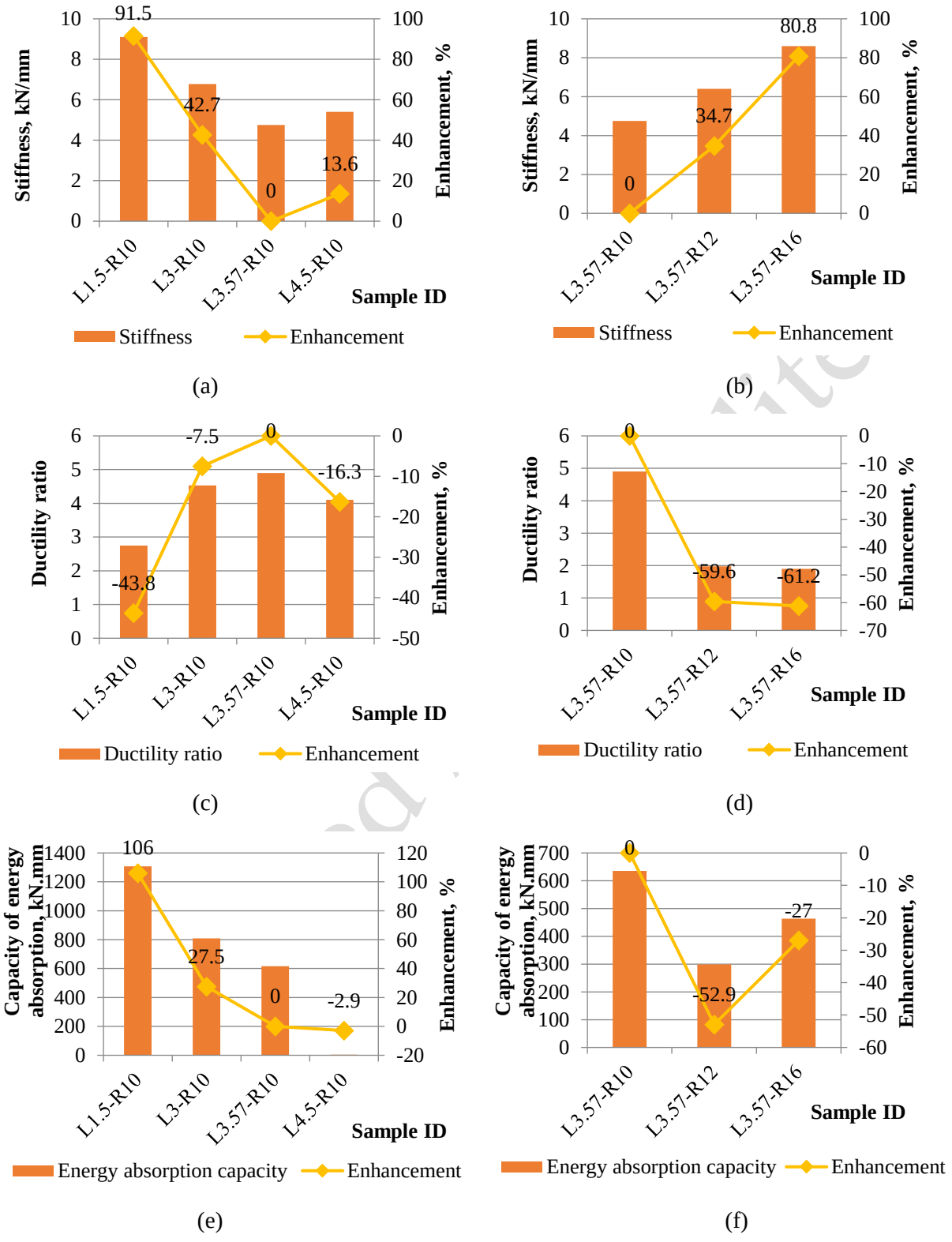

Fig. 7 Enhancement percentage: (a) Stiffness of various shear-span depth ratio samples. (b) Stiffness of the samples with various reinforcement ratios. (c) Ductility of samples with various shear-span depth ratios. (d) Ductility of various reinforcement ratio samples. (e) Capacity of energy absorption for samples with various shear-span depth ratios. (f) Energy absorption capacities of the samples with various reinforcement ratios.

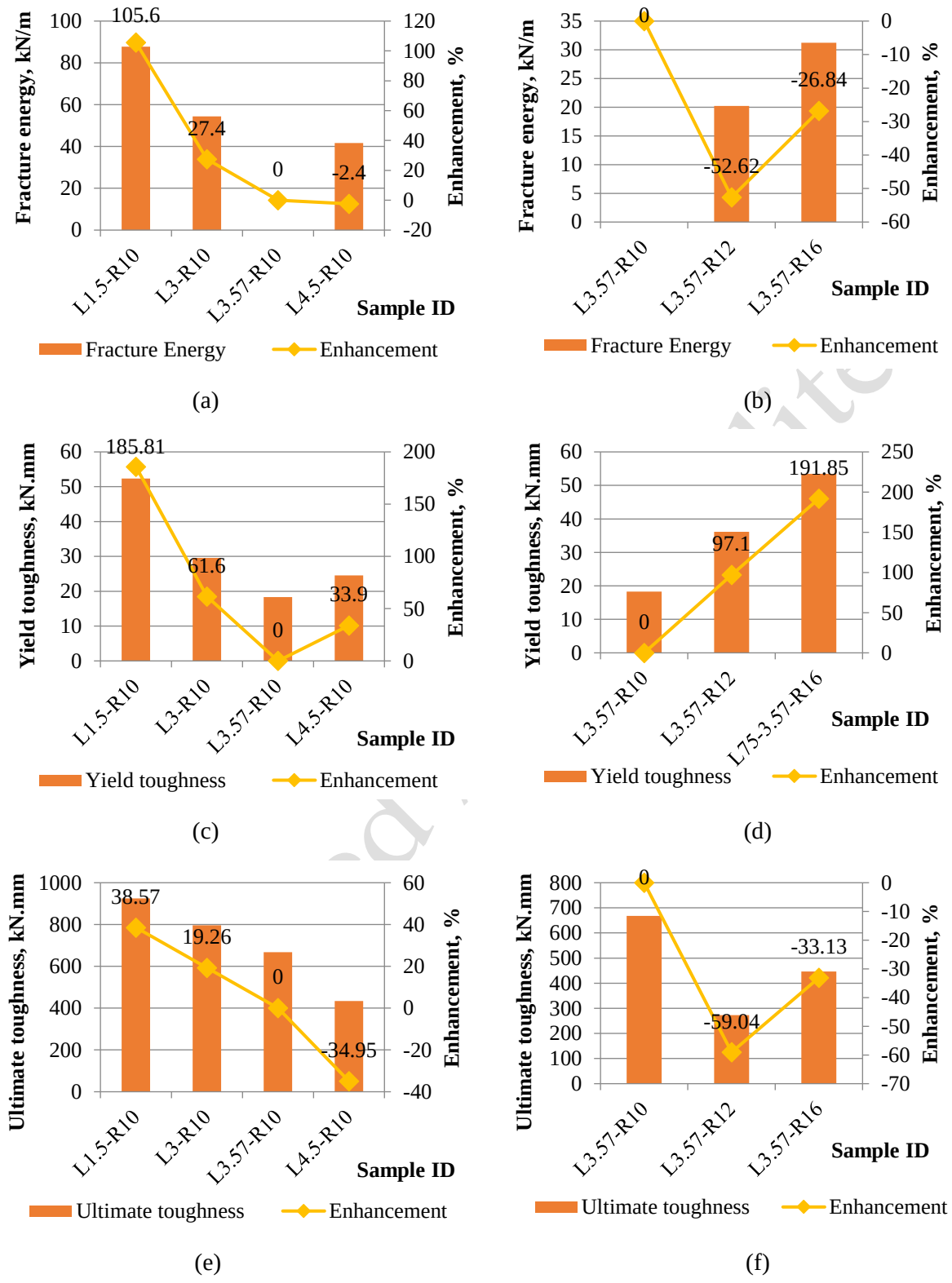

Fig. 8 Enhancement percentage of: (a) Fracture energy at various shear-span depth ratios. (b) Fracture energies at various reinforcement ratios. (c) Yield toughness at various shear-span depth ratios. (d) Yield toughness at various reinforcement ratios. (e) Ultimate toughness at various shear-span depth ratios. (f) Ultimate toughness at various reinforcement ratios.

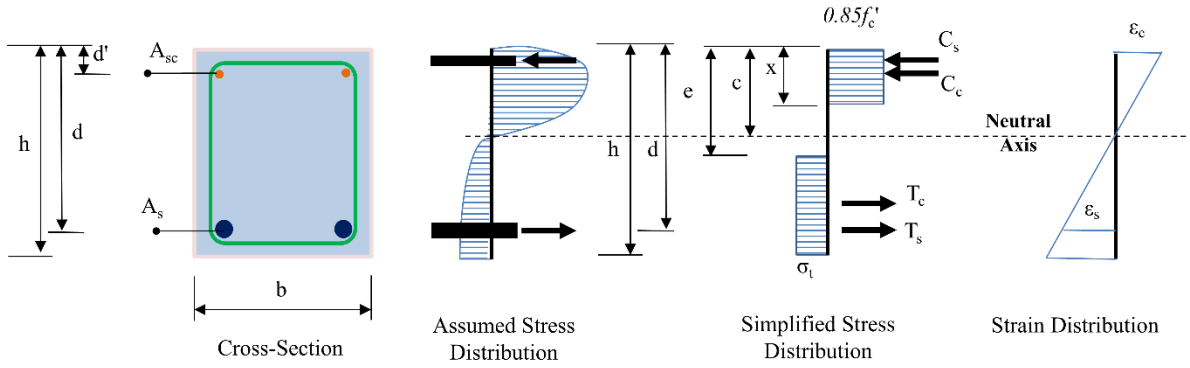

Fig. 9 Design assumptions for reinforced fibrous concrete beams.

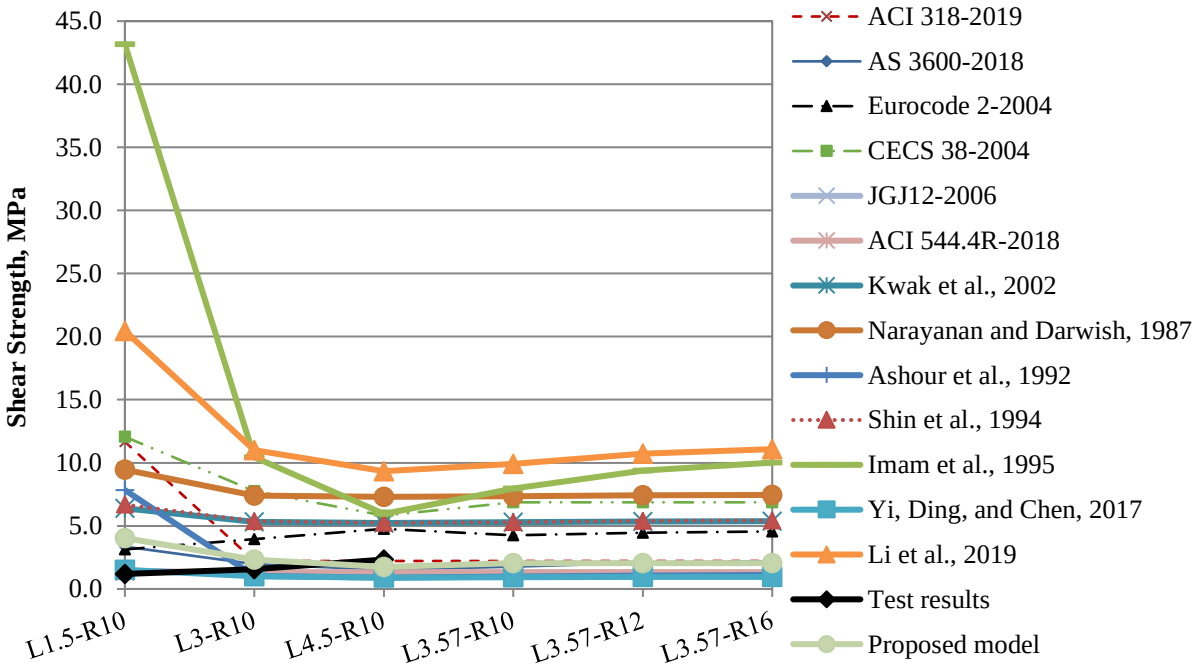

Fig. 10 Shear strength results and values predicted using theoretical and experimental models.

List of Tables

Table 1 Concrete mixtures for the research samples (kg/m^3).

Materials	Quantity
Cement	500
Water	195
Sand	574.4
Dolomite	248.9
LECA	484.5
Silica Fume	40
High Range Water Reducer	11
Glass fiber (% of volume)	2%

Table 2 Sieve analysis of study aggregate types.

Particle size (mm)	% Passing		
	Fine Aggregate	Coarse Aggregate	LECA
20	-	-	95.9
14	-	99.2	19.7
10	-	77.6	-
5	99.4	12.5	-
2.36	95	-	-
1.18	87.4	-	-
0.6	44.4	-	-
0.3	8.6	-	-
0.15	2	-	-

Table 3 Physical and mechanical properties of concrete mixes.

LECA content	Density			Slump		Compression strength			Strength/weight ratio (MPa/kg)	Split tensile strength		
	Mean kg/m^3	SD	Change %	mm	Change %	Mean kg/m^3	SD	Change %		Mean kg/m^3	SD	Change %
0%	2419	17	-	60	-	48.41	1.26	-	5.05	3.40	0.28	-
75%	2028	28	-16	80	+33	31.13	0.31	-35	3.46	1.58	0.18	-53
85%	1986	130	-17	93	+55	28.21	1.67	-41	2.85	1.82	0.15	-46
95%	1930	81	-20	105	+75	25.68	3.43	-46	2.71	2.03	0.08	-40

Table 4 Details of test beam samples.

Beam determination	Shear-span depth ratio, a/d	Beam size, b×d (mm)	Tension reinforcement		
			Number and size	As, (mm^2)	ρ = As\bd (%)
L3.57-R10 (control)	3.57	100×150	2Φ10	157	1.04
L1.5-R10	1.5				
L3-R10	3				
L4.5-R10	4.5				
L3.57-R12	3.57		2Φ12	204	1.36
L3.57-R16	3.57		2Φ16	226	1.5

Table 5 Load, moment resistance capacity, displacement, and collapse modes of samples with different shear-span depth ratios and reinforcement ratios at the cracking and peak stages.

Sample ID	Cracking stage			Peak stage			Collapse mode
	Cracking load (kN)	Cracking moment resistance (kN.m)	Displacement at cracking load, Δ_{cr} (mm)	Maximum load (kN)	Maximum moment resistance (kN.m)	Displacement at maximum load, Δ_{max} (mm)	
L3.57-R10	13.00	3.25	2.818	33.35	8.34	10.34	Flexural-Compression
L1.5-R10	32.00	8.00	3.272	80.59	20.15	16.11	Shear-Compression
L3-R10	20.05	5.02	2.953	44.51	11.13	12.28	Flexural-Compression
L4.5-R10	16.20	4.05	3.028	32.36	8.09	10.76	Flexural-Compression
L3.57-R16	30.10	7.53	3.552	65.27	16.31	10.02	Shear-Compression
L3.57-R12	21.30	5.33	3.390	43.56	10.89	9.65	Shear-Compression

Table 6 Mean, standard deviation, and coefficient of variation of the ratios of the theoretical values of shear strength of FLC beams calculated by each model $v_{fc;THEO}$ to their experimental values $v_{fc;EXP}$.

Model	Mean value of $v_{fc;THEO}/v_{fc;EXP}$	Standard deviation SD of $v_{fc;THEO}/v_{fc;EXP}$	Coefficient of Variation CV (%)
Proposed model	0.93	0.37	39.64
ACI 318-2019	1.36	0.38	27.94
AS 3600-2018	0.92	0.42	45.57
Eurocode 2-2004	1.76	1.22	69.21
CECS 38-2004	3.04	1.33	43.74
JGJ12-2006	0.48	0.25	53.03
ACI 544.4R-2018	0.54	0.33	60.46
Kwak et al., 2002	2.23	1.25	56.38
Narayanan and Darwish, 1987	3.12	1.70	54.47
Ashour et al., 1992	0.77	0.34	44.98
Shin et al., 1994	2.26	1.25	55.23
Imam et al., 1995	5.54	1.09	19.66
Yi et al., 2017	0.42	0.20	47.35
Li et al., 2019	4.87	1.95	40.06